

Efficient algorithms for semiclassical instanton calculations based on discretized path integrals

メタデータ	言語: eng 出版者: 公開日: 2017-10-03 キーワード (Ja): キーワード (En): 作成者: メールアドレス: 所属:
URL	https://doi.org/10.24517/00010844

This work is licensed under a Creative Commons Attribution-NonCommercial-ShareAlike 3.0 International License.



Efficient algorithms for semiclassical instanton calculations based on discretized path integrals

Tsutomu Kawatsu and Shinichi Miura

Citation: *The Journal of Chemical Physics* **141**, 024101 (2014); doi: 10.1063/1.4885437

View online: <http://dx.doi.org/10.1063/1.4885437>

View Table of Contents: <http://scitation.aip.org/content/aip/journal/jcp/141/2?ver=pdfcov>

Published by the [AIP Publishing](#)

Articles you may be interested in

[Coupled-cluster study of the electronic structure and energetics of tetrasulfur, S₄](#)

J. Chem. Phys. **127**, 174305 (2007); 10.1063/1.2774973

[A calculation of the rovibronic energies and spectrum of the B¹ A₁ electronic state of SiH₂](#)

J. Chem. Phys. **123**, 244312 (2005); 10.1063/1.2139676

[Geometry and spin-multiplicity of half-sandwich type transition-metal-benzene complexes](#)

J. Chem. Phys. **122**, 134303 (2005); 10.1063/1.1867434

[Intermolecular potential for the interaction of helium with ammonia](#)

J. Chem. Phys. **114**, 8836 (2001); 10.1063/1.1367379

[Structure and vibrational dynamics of the benzene dimer](#)

J. Chem. Phys. **111**, 572 (1999); 10.1063/1.479338



AIP | Journal of
Applied Physics

Journal of Applied Physics is pleased to
announce **André Anders** as its new Editor-in-Chief

Efficient algorithms for semiclassical instanton calculations based on discretized path integrals

Tsutomu Kawatsu^{1,2,a)} and Shinichi Miura^{2,a)}

¹*Institute for Molecular Science, National Institute of Natural Science, 38 Nishigonaka, Myodaiji, Okazaki 222-8585, Japan*

²*School of Mathematics and Physics, Kanazawa University, Kanazawa 920-1192, Japan*

(Received 28 March 2014; accepted 16 June 2014; published online 8 July 2014)

Path integral instanton method is a promising way to calculate the tunneling splitting of energies for degenerated two state systems. In order to calculate the tunneling splitting, we need to take the zero temperature limit, or the limit of infinite imaginary time duration. In the method developed by Richardson and Althorpe [J. Chem. Phys. **134**, 054109 (2011)], the limit is simply replaced by the sufficiently long imaginary time. In the present study, we have developed a new formula of the tunneling splitting based on the discretized path integrals to take the limit analytically. We have applied our new formula to model systems, and found that this approach can significantly reduce the computational cost and gain the numerical accuracy. We then developed the method combined with the electronic structure calculations to obtain the accurate interatomic potential on the fly. We present an application of our *ab initio* instanton method to the ammonia umbrella flip motion. © 2014 AIP Publishing LLC. [<http://dx.doi.org/10.1063/1.4885437>]

I. INTRODUCTION

The tunneling effect often plays an important role to describe molecular processes occurred in chemical and biological systems^{1–3} as well as fundamental physical processes.^{4,5} The experimental observable concerning the effect is the energy difference of nearly degenerate ground and first excited states of the system, which is called the tunneling splitting. The path integral Monte Carlo or molecular dynamics method^{6–9} and the diffusion Monte Carlo method^{10–14} provide exact numerical approaches to calculate the tunneling splitting. However, these methods usually need high computational cost because extensive sampling is required to accurately estimate the tunneling splitting. On the other hand, the path integral instanton approach has been developed as a method for approximate path integral calculations, which dramatically reduces the computational cost compared with the exact numerical approaches,^{4,5,15–44} including the evaluation of the tunneling splitting.^{4,5,23–44} Instead of massive samplings over whole possible paths, the instanton method is formulated on the basis of the steepest descent approximation regarding the associated partition function. In this approximation, classical paths connecting equilibrium states, which minimize an imaginary time action of the system considered, and second order fluctuation orthogonal to each classical path are incorporated to derive the expression of the tunneling splitting. In numerical applications, a classical path traveling once from a minimum to another minimum, which is called single kink path, must be calculated accurately. To obtain the reliable single kink path, several variants on the least action approach have been proposed.^{20,21,35–45} To describe the sin-

gle kink path, the action is expressed using the discretized imaginary time axis^{18–21,39–45} as well as using the continuous time axis.^{15–17,22–38} In the present paper, we focus a method using the discretized imaginary time approach developed by Richardson and Althorpe, because their method is constructed on the basis of the standard path integral molecular simulation technology, which facilitates the reuse of existing computational libraries on the path integrals.^{41,42} Then, the single kink path is computed by minimizing the potential energy of isomorphic polymers with a proper boundary condition.^{41,42}

Using the instanton method with the discretized path integral approach, we have to take the zero temperature limit, or the infinity limit of the imaginary time duration $\beta\hbar$ together with vanishing limit of the imaginary time step $\Delta\tau$. In the Richardson-Althorpe's formula, these limits with respect to $\beta\hbar$ and $\Delta\tau$ are replaced to be large and small enough values, respectively. In our previous study, we have developed a method to extend $\beta\hbar$ simply by adding the copies of the system at each local state to both ends of the single kink path, which results in the reduction of the computational cost.⁴³ In the present paper, we have extended our previous method to take the limit of the infinite $\beta\hbar$ analytically.

In the path integral instanton method, the tunneling splitting is written as an exponential of a single kink action which is very sensitive to the accuracy of the potential function. To evaluate the tunneling splittings on the accurate potential energy surface, we have developed a method combining our efficient algorithm of the path integral instanton approach with the *ab initio* molecular orbital theory. We applied our method to tunneling splittings of ammonia umbrella flip motions. The ammonia flips are well studied and the tunneling splittings for these isotopomers have been measured experimentally. The tunneling splitting for the ground state have been measured in microwave spectroscopies as 0.793 cm^{-1} .^{46,47} The

^{a)}Authors to whom correspondence should be addressed. Electronic addresses: kawatsu@fukui.kyoto-u.ac.jp and smiura@mail.kanazawa-u.ac.jp.

tunneling splittings are also calculated using various theoretical approaches.^{28,34,48–51} We have obtained quantitative agreements to these measurements in our calculations.

This paper is organized as follows: In Sec. II A, we summarize the formulation by Richardson and Althorpe. Then, we derive the expression of the tunneling splitting for the infinite $\beta\hbar$ using a single kink path in a finite imaginary time duration in Sec. II B. We tested our new formula to a one-dimensional system in Sec. II C. The formula is extended to general three-dimensional systems in Secs. III A and III B. The computational results are presented in Sec. III C. Then, we demonstrate our method combined with *ab initio* electronic structure calculations in Sec. IV. We conclude in Sec. V.

II. PATH INTEGRAL FORMULATION OF TUNNELING SPLITTINGS

A. Summary of Richardson-Althorpe's theory

At the beginning, we summarize the formulation of the tunneling splittings using the instanton approach by Richardson and Althorpe.⁴¹ In Sec. II, we consider one-dimensional double-well systems for simplicity. Multi-dimensional extensions will be discussed in later sections. In the standard ring-polymer approach, a partition function of the one-dimensional system at an inverse temperature β is written as¹⁸

$$Z(\beta) = \text{Tr} e^{-\beta\hat{H}} = \lim_{P \rightarrow \infty} \left(\frac{P}{2\pi\beta\hbar^2} \right)^{\frac{P}{2}} \int \cdots \int \left(\prod_{s=1}^P dq^{(s)} \right) \times e^{-\beta W(\{q^{(s)}\}; \beta)}, \quad (1)$$

where $q^{(s)} \equiv \sqrt{m} \times$ (position at an imaginary time slice s) is the mass-scaled coordinate of a particle with mass m and P is the number of imaginary time slices. In this expression, whole imaginary time duration $\beta\hbar$ is discretized into P short time steps with an equal step size $\Delta\tau \equiv \beta\hbar/P$. An effective interaction W is written by

$$W(\{q^{(s)}\}; \beta) = \sum_{s=1}^P \frac{1}{2} \omega_p^2 (q^{(s)} - q^{(s+1)})^2 + \frac{1}{P} \sum_{s=1}^P V(q^{(s)}), \quad (2)$$

where $\omega_p \equiv \sqrt{P}/\beta\hbar$ and $V(q)$ is a potential energy of the system considered, which is isomorphic with a classical ring polymer of P interaction sites. In the instanton method, we apply the steepest descent approximation to evaluate the multidimensional integral in Eq. (1). Then, the partition function is approximated to be

$$Z(\beta) \approx \tilde{Z}(\beta) = \lim_{P \rightarrow \infty} \left(\frac{P}{2\pi\beta\hbar^2} \right)^{\frac{P}{2}} \sum_{\text{minima}} \sqrt{\frac{2\pi\hbar}{\det G}} e^{-\beta W(\{\tilde{q}^{(s)}\}; \beta)}, \quad (3)$$

where G is a second-derivative of W . The symbol $\{\tilde{q}^{(s)}\}$ represents a set of coordinates of a minimum effective interaction path connecting two classical equilibrium states. Equation (3) includes contributions from the minimum energy paths and harmonic fluctuations along these paths. The summation in Eq. (3) is taken over all minimum energy paths. Here, we classify the minimum energy paths using the number

of transitions between two equilibrium states. We call a single transition between equilibrium states a kink. In the instanton method, the multiple kink paths are expressed by the single kink path using a kink gas approximation. Using a partition function $\tilde{Z}_0(\beta)$ corresponding to a non-tunneling system, the partition function is analytically expressed to be

$$\frac{\tilde{Z}(\beta)}{\tilde{Z}_0(\beta)} = \cosh(P\theta(\beta)), \quad (4)$$

where $\theta(\beta)$ only includes a single kink contribution, which is written as

$$\theta(\beta) = \frac{\beta\hbar}{P\Phi} \sqrt{\frac{S_{\text{kink}}}{2\pi\hbar}} e^{-\frac{S_{\text{kink}}}{\hbar}} \quad (5)$$

and

$$\Phi = \sqrt{\frac{\det' J_{\text{kink}}}{\det J_0}}, \quad (6)$$

where $S_{\text{kink}} \equiv \beta\hbar W(\{\tilde{q}^{(s)}\}; \beta)$ is a single kink action, and J_0 and J_{kink} are second derivative of the zero and single kink actions divided by $\Delta\tau = \beta\hbar/P$, respectively. The symbol \det' in Eq. (6) indicates a determinant without a zero eigenvalue mode associated with the translation of the kink in the imaginary time; the mode yields the factor of $\sqrt{S_{\text{kink}}/2\pi\hbar}$ in Eq. (5). On the other hand, the partition function of degenerated two-state systems is exactly written using the tunneling splitting $\Delta\varepsilon$ as

$$\lim_{\beta \rightarrow \infty} \frac{Z(\beta)}{Z_0(\beta)} = \cosh\left(\frac{\beta\Delta\varepsilon}{2}\right). \quad (7)$$

Comparing Eq. (4) with Eq. (7), we reach the expression of the tunneling splitting as

$$\Delta\varepsilon \approx \lim_{\beta \rightarrow \infty, P \rightarrow \infty} 2\frac{P}{\beta}\theta(\beta). \quad (8)$$

We rename $P \rightarrow \infty$ limit to $\Delta\tau \rightarrow 0$ for later convenience. The final expression of the tunneling splitting is written by

$$\Delta\varepsilon \approx \lim_{\beta \rightarrow \infty, \Delta\tau \rightarrow 0} \frac{2\hbar}{\Phi} \sqrt{\frac{S_{\text{kink}}}{2\pi\hbar}} e^{-S_{\text{kink}}/\hbar}. \quad (9)$$

To numerically evaluate the tunneling splitting using Eq. (9), we adopt a finite β that is large enough, and $\Delta\tau = \beta\hbar/P$ is short enough. We also need to find a single kink path connecting two equilibrium states. We introduce an open chain polymer consisting of $M+1$ interaction sites, or time slices according to the procedure by Richardson and Althorpe. Then, the single kink path is obtained by minimizing the effective interaction of the open chain polymer W by the following relation:

$$\frac{\partial W(q^{(0)}, \dots, q^{(M)}; \beta)}{\partial q^{(s)}} = 0, \quad (s = 1, 2, \dots, M-1) \quad (10)$$

with the boundary conditions where the configurations at the end time slices, $q^{(0)}$ and $q^{(M)}$, are fixed at the equilibrium states, respectively. Here, the number of time slices M does not need to equal with P , actually, M must be determined by the condition that a β is large enough and a $\Delta\tau = \beta\hbar/M$ is small enough to accurately describe a single transition path.

In the present paper, we extend the formula of Eqs. (6) and (9) to analytically take an infinity limit of β .

B. Fluctuation determinant for one-dimensional system in the infinite β

At the beginning of this subsection, we would like to point out two important features of the single kink path for the following discussions. First, when β is long enough to form a kink in the imaginary time, the local structure around the kink does not change even if β is lengthened further.⁴³ Second, we consider the situation that each end of the path, which consists of $L - 1$ imaginary time slices, stays in each minimum of the potential energy. Namely, if we have an isomorphic polymer longer than $L - 1$ in this situation with a given $\Delta\tau$, the rest of imaginary time slices at each end of the polymer stay in the minimum $q^{(0)}$ and $q^{(M)}$.⁴³ We consider an operation to decompose such long isomorphic polymer with a length $\beta\hbar = \Delta\tau(2L_0 + L - 1)$ into a part of $L - 1$ imaginary time slices with a single kink and L_0 copies of imaginary time slices in each local minimum at these ends of the path. Using $V(q^{(0)}) = V(q^{(M)}) = 0$, it is trivial that S_{kink} is independent of the size of L_0 . Therefore, only Φ factor depends on β value

in Eq. (9) for this operation. Thus, we focus on the Φ factor, Eq. (6), to develop our method. The Φ factor is defined using J_{kink} and J_0 . According to the above observations, each matrix could be decomposed into submatrices related with a part of $L - 1$ time slices and with two parts of L_0 time slices. The point is that after the above decomposition, making β longer is only related with the number L_0 . In the following, we develop a rational decomposition of J_{kink} and J_0 to efficiently take the infinite β limit.

First, we consider J_{kink} that is a Hessian matrix of the $S_{\text{kink}}/\Delta\tau$ evaluated along the single kink path. Here, we introduce a notation regarding a matrix X ; hereafter, we write an element of the matrix X as $X[x, y]$, where x and y indicate row and column in X , respectively. Because configurations at 0th and M th imaginary time slices are fixed at the equilibrium structures, J_{kink} is a $(M - 1) \times (M - 1)$ matrix. The $M - 1$ time slices are classified into three parts; first L_0 time slices associated with an equilibrium state, the following $L - 1$ time slices with the kink, and L_0 time slices with another equilibrium state; $M - 1 = 2L_0 + L - 1$. We denote the second derivatives at the first and last equilibrium states to be h_0 and h_L , respectively. Then, the elements $J_{\text{kink}}[i, j]$ are written as

$$J_{\text{kink}}[i, j] = \begin{cases} a_0 \equiv h_0 + 2c & (i = j, 1 \leq i \leq L_0) \\ a_m \equiv h_m + 2c & (m = i - L_0, i = j, L_0 + 1 \leq i \leq L_0 + L - 1) \\ a_L \equiv h_L + 2c & (i = j, L_0 + L \leq i \leq 2L_0 + L - 1) \\ -c & (i = j \pm 1) \\ 0 & (\text{others}) \end{cases}, \quad (11)$$

where indices i and j run from 1 to $M - 1$ and a constant $c \equiv \Delta\tau^{-2}$. The symbol h_m denotes the second derivative of the system at an imaginary time defined above. We have defined a_0 , a_m , and a_L to make expressions compact. Since we are considering a symmetric transition system that two local states have the same second derivative, $a_0 = a_L$ whose value is positive, because h_0 is for the equilibrium state and $c > 0$.

We next rewrite the matrix J_{kink} without changing the value of the determinant as follows. We apply the method of Gaussian elimination to J_{kink} to delete lower off-diagonal components of first $L_0 - 1$ and last $L_0 - 1$ columns. Adding (m th line \times its diagonal element $\times c$) to ($m + 1$)th line, and repeating the operation from $m = 1$ to $L_0 - 1$, then, lower off-diagonal elements of first $L_0 - 1$ columns vanish. Similarly, adding (m th column \times its diagonal element $\times c$) to ($m - 1$)th column, and repeating the operation from $m = M - 1$ to $M - L_0 - 1$, then, lower off-diagonal elements of last $L_0 - 1$ columns are also removed. Upper off-diagonal elements can be deleted as well. Then, the determinant of J_{kink} can be written as

$$\det J_{\text{kink}} = \begin{vmatrix} \bar{B} & O & O \\ O & J'_{\text{kink}} & O \\ O & O & \underline{B} \end{vmatrix}, \quad (12)$$

where $(L + 1) \times (L + 1)$ matrix J'_{kink} is defined by

$$J'_{\text{kink}}[k, l] \equiv \begin{cases} b_{L_0} & (k = l, k = 0 \text{ or } L) \\ a_k & (k = l, 0 < k < L) \\ -c & (k = l \pm 1) \\ 0 & (\text{others}) \end{cases}, \quad (13)$$

where indices k and l run from 0 to L . \bar{B} and \underline{B} are $(L_0 - 1) \times (L_0 - 1)$ diagonal matrices, and these diagonal elements are $\bar{B}[m, m] \equiv b_m$ and $\underline{B}[m, m] \equiv b_{L_0 - m}$, respectively. The symbol O indicates a zero matrix. The process of the Gaussian elimination yields the following recurrence relation of b_m :

$$b_m = h_0 + 2c - c^2 \frac{1}{b_{m-1}}. \quad (14)$$

The solution of the above recurrence relation is described in Appendix A. The solution Eq. (A6) in the case of $h_0 \neq 0$ with the initial value $b_1 = h_0 + 2c$ is written as

$$b_m = \frac{\alpha_+ - \alpha_- D^m}{1 - D^m}, \quad (15)$$

where α_{\pm} are defined as

$$\alpha_{\pm} \equiv \frac{1}{2}(h_0 + 2c \pm \sqrt{(h_0)^2 + 4ch_0}), \quad (16)$$

and $D \equiv \alpha_-/\alpha_+$. Because D is always smaller than 1,

$$b_{\infty} = \alpha_+. \quad (17)$$

It is worthwhile to note that Eq. (17) does not depend on the initial value of the recurrence relation, b_1 . Since \bar{B} and \underline{B} are diagonal matrices as stated above, the determinant of J_{kink} , Eq. (12), can be expressed as

$$\det J_{\text{kink}} = \det J'_{\text{kink}} \prod_{m=1}^{L_0-1} (b_m)^2. \quad (18)$$

On the other hand, we apply similar operations to $\det J_0$ associated with the non-tunneling system. The elements of original $(M-1) \times (M-1)$ matrix J_0 are written by

$$J_0[i, j] = \begin{cases} a_0 & (i = j) \\ -c & (i = j \pm 1) \\ 0 & (\text{others}) \end{cases}. \quad (19)$$

Then, we obtain analytical form of $\det J_0$ as

$$\det J_0 = \prod_{m=1}^{M-1} b_m. \quad (20)$$

However, instead of Eq. (20), we here employ similar form to Eq. (18) to express $\det J_0$:

$$\det J_0 = \det J'_0 \prod_{m=1}^{L_0-1} (b_m)^2 \quad (21)$$

and

$$J'_0[k, l] \equiv \begin{cases} b_{L_0} & (k = l, k = 0 \text{ or } L) \\ a_0 & (k = l, 0 < k < L) \\ -c & (k = l \pm 1) \\ 0 & (\text{others}) \end{cases}. \quad (22)$$

Dividing Eq. (18) by Eq. (21), we obtain the following relation:

$$\frac{\det J_{\text{kink}}}{\det J_0} = \frac{\det J'_{\text{kink}}}{\det J'_0}. \quad (23)$$

Equation (23) indicates that the ratio of the determinants $\det J_{\text{kink}}$ and $\det J_0$ can be expressed using determinants of smaller $(L+1) \times (L+1)$ matrices, $\det J'_{\text{kink}}$ and $\det J'_0$, and the eigenvalues of \bar{B} and \underline{B} are totally canceled out. Then, we consider the limit of $\beta \rightarrow \infty$. This limit corresponds to $L_0 \rightarrow \infty$. Since this operation only affects the matrix element b_{L_0} , the expression at $L_0 \rightarrow \infty$ limit of Eqs. (13) and (22) is given by the following replacement: $b_{L_0} \rightarrow b_{\infty}$. Namely, we obtain our equation for infinite-size full-path matrices, J_{kink} and J_0 , using finite-size local-path matrices, J''_{kink} and J''_0 . Then, the infinite β limit of Eq. (23) is written by

$$\lim_{\beta \rightarrow \infty} \frac{\det J_{\text{kink}}}{\det J_0} = \frac{\det J''_{\text{kink}}}{\det J''_0}, \quad (24)$$

where local path matrices are defined to be

$$J''_{\text{kink}}[k, l] \equiv \lim_{L_0 \rightarrow \infty} J'_{\text{kink}}[k, l] = \begin{cases} b_{\infty} & (k = l, k = 0 \text{ or } L) \\ J'_{\text{kink}}[k, l] & (\text{others}) \end{cases} \quad (25)$$

and

$$J''_0[k, l] \equiv \lim_{L_0 \rightarrow \infty} J'_0[k, l] = \begin{cases} b_{\infty} & (k = l, k = 0 \text{ or } L) \\ J'_0[k, l] & (\text{others}) \end{cases}, \quad (26)$$

where b_{∞} is given in Eq. (17). As in the Richardson-Althorpe method, a zero eigenvalue mode related with the translation of the kink in the imaginary time is handled separately, see Eq. (6). New formula of the Φ factor in the infinite β is written as

$$\lim_{\beta \rightarrow \infty} \Phi = \left(\frac{\det' J''_{\text{kink}}}{\det J''_0} \right)^{\frac{1}{2}}. \quad (27)$$

Our formula can simply be obtained by replacing two elements a_0 and a_L in Eq. (6) by b_{∞} . However, the resulting formula is the expression at the infinite β limit for Eq. (9). The numerical application of Eq. (27) is demonstrated in Subsection II C.

C. Numerical application to a one-dimensional system

In this subsection, we present an application of our new formula to a one-dimensional system based on Eq. (27). To obtain the single kink path, we have used a discretized path integral expression of a propagator from an equilibrium state to another equilibrium state to clarify the order of discretization error and facilitate the use of higher order formula. Using the second-order Suzuki-Trotter formula $e^{-\hat{H}\Delta\tau} = e^{-\hat{V}\Delta\tau/2} e^{-\hat{T}\Delta\tau} e^{-\hat{V}\Delta\tau/2} + O(\Delta\tau^3)$,⁵² the propagator from $-q_0$ to q_0 is written as

$$\langle -q_0 | e^{-\beta\hat{H}} | q_0 \rangle = \int \cdots \int \left(\prod_{s=1}^{M-1} dq^{(s)} \right) e^{-\beta W(\{q^{(s)}\}; \beta)}, \quad (28)$$

and the effective interaction W is re-defined as

$$W(\{q^{(s)}\}; \beta) \equiv \sum_{s=0}^{M-1} \frac{1}{2} \omega_M^2 (q^{(s)} - q^{(s+1)})^2 + \frac{1}{M} \left(\sum_{s=1}^{M-1} V(q^{(s)}) + \frac{1}{2} (V(q^{(0)}) + V(q^{(M)})) \right), \quad (29)$$

where the coordinates $q^{(0)} = -q_0$ and $q^{(M)} = q_0$ are fixed at two degenerated local states, respectively. The effective interaction W corresponds to the system of a linear polymer consisting of $M+1$ interaction sites whose ends are fixed at $-q_0$ and q_0 .

Here, instead of β , we use a parameter $\beta_L \equiv L\Delta\tau/\hbar$ to specify the imaginary time duration for Eq. (28). In our computational studies, we used L-BFGS subroutine^{53,54} for optimizing the isomorphic open polymer to find the stationary path, and LAPACK library for the diagonalization of matrices. In the course of the calculations, we have optimized

whole polymer coordinates including $q^{(0)}$ and $q^{(M)}$ to find the single kink path, instead of Eq. (10), according to the procedure described in Ref. 41.

We adopted the following potential function as a one-dimensional double well system:

$$V(x) = V_0 \left(\frac{x^2}{x_0^2} - 1 \right)^2. \quad (30)$$

The equilibrium states are located at $x = \pm x_0$, and the potential barrier is V_0 . In the present model, the parameters $a_0 (= a_L)$ and b_∞ are analytically evaluated by

$$a_0 = \frac{8V_0}{x_0^2} + 2c \quad (31)$$

and

$$b_\infty = \frac{4V_0}{x_0^2} + c + \sqrt{\frac{16V_0^2}{x_0^4} + \frac{8V_0c}{x_0^2}}, \quad (32)$$

respectively. The new formula (27) is obtained by replacing a_0 in the Φ factor in the Richardson-Althorpe's formula (9) by b_∞ .

Figure 1 shows computational results of the tunneling splitting $\Delta\varepsilon$ for various β_L with fixed $\Delta\tau = 0.1$, together with results of the Richardson-Althorpe's formula. To compare our results with Richardson-Althorpe's calculations, we adopted the same parameter, $V_0 = 1.0$ and $x_0 = 5.0$, of their paper.⁴¹ We show the results for $\beta_L\hbar$ ranging from 22 to 60 in Fig. 1. In Fig. 1, we find an improvement of the numerical result in the time region around $\beta_L\hbar = 25\text{--}40$. Actually, our new method can obtain the same quality of the result by 40 imaginary time slices using only 25 time slices. It is worth noting that generally the computational cost of the potential and Hessian calculations of isomorphic polymer is proportional to the number of time slices. It is noted that these differences are smaller than significant figures presented in Ref. 41. When the $\beta_L\hbar$ value is larger than 60, two methods give the same converged result, which means that b_{L_0} numerically equals b_∞ , see Eqs. (13) and (25). In fact, b_m converges very fast regarding m , see Eq. (15) and $D \approx 0.88$. Since, in the present study, the discretized path integral expression is constructed

by the second order Suzuki-Trotter formula, our formula may depend on $\Delta\tau$ as follows:

$$\Delta\varepsilon(\Delta\tau) \approx \Delta\varepsilon(0) + C\Delta\tau^2, \quad (33)$$

where $\Delta\tau$ is small enough and C is a constant. It is commented that our new formula guarantees that for any $\Delta\tau$ computed values of the tunneling splitting has no β_L dependent unless β_L is too short to describe the single kink path. We then computed tunneling splittings using various small $\Delta\tau$ and applied a least square fitting to numerical results. Then, the final result for tunneling splitting is obtained as y-intercept of the fitted curve. We show the computed results of tunneling splitting and the fitted curve in Fig 1. The final value of the tunneling splitting is obtained to be 3.861×10^{-4} , which agrees well with the Richardson-Althorpe's result.

III. EXTENSION TO MULTIPLE DIMENSIONS

In Sec. II, we have introduced a formula to express Φ factor at $\beta \rightarrow \infty$ limit using finite size matrices. In this section, we extend the formula to handle molecular systems in three-dimensional Cartesian space.

A. Fluctuation determinant for molecular systems in the infinite β

We first reformulate Eq. (27) for molecular systems in three-dimensional Cartesian space. For such cases, an element of matrix in Sec. II becomes a $3N \times 3N$ matrix, where N is the number of atoms in the system. To express our formula for three-dimensional systems as similar to Sec. II, we write a $3NM \times 3NM$ matrix X , where M is the number of associated imaginary time slices, using $3N \times 3N$ submatrices as follows. The matrix X is divided into $3N \times 3N$ matrices, each partial matrix specified by a notation of $X[x, y]$, where x and y indicate the labels of corresponding imaginary time slices.

Partial matrices $J_{\text{kink}}[i, j]$ of $3N(M-1) \times 3N(M-1)$ matrix J_{kink} are written by

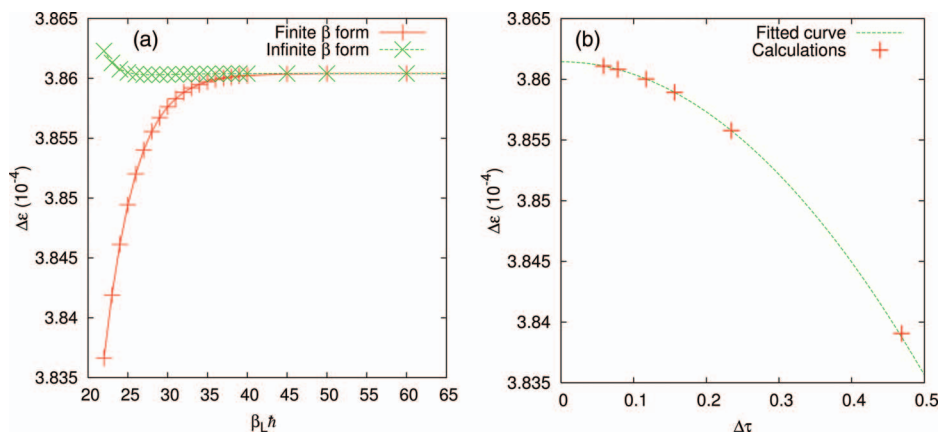


FIG. 1. (a) Tunneling splitting $\Delta\varepsilon$ calculated by the Richardson-Althorpe's form (finite β form) and by new form (infinite β form) in a one-dimensional system. Curve is drawn as a guide to eye. (b) Tunneling splittings for various $\Delta\tau$ for $\beta_L\hbar = 60$. A curve is obtained by a least square fitting of computed tunneling splittings for the data $\Delta\tau < 0.4$.

$$J_{\text{kink}}[i, j] = \begin{cases} A_0 \equiv H_0 + 2cI_{3N} & (i = j, 1 \leq i \leq L_0) \\ A_m \equiv H_m + 2cI_{3N} & (i = j, m = i - L_0, L_0 + 1 \leq i \leq L_0 + L - 1) \\ A_L \equiv H_L + 2cI_{3N} & (i = j, L_0 + L \leq i \leq 2L_0 + L) \\ -cI_{3N} & (i = j \pm 1) \\ O & (\text{others}) \end{cases}, \quad (34)$$

where H_0 and H_L are the Hessian matrix of the molecular systems at corresponding equilibrium states, respectively, H_m is the Hessian matrix of the systems at an imaginary time slice defined above, I_n is an $n \times n$ identity matrix, and O is zero matrix. The notations for the numbers of imaginary time slices, M , L , and L_0 are the same as in Sec. II. We consider an orthogonal matrix U_0 to diagonalize the Hessian H_0 . We write n th eigenvalue of H_0 to be η_0^n . The matrix U_0 also diagonalizes the matrix A_0 whose eigenvalue is $\eta_0^n + 2c$. Similarly, the matrix U_L and the related eigenvalue η_L^n are introduced. We next define the following $3N(M-1) \times 3N(M-1)$ matrix U' with partial matrix elements $U'[i, j]$:

$$U'[i, j] \equiv \begin{cases} U_0 & (i = j, 1 \leq i \leq L_0) \\ I_{3N} & (i = j, L_0 + 1 \leq i \leq L_0 + L - 1) \\ U_L & (i = j, L_0 + L \leq i \leq 2L_0 + L) \\ O & (\text{others}) \end{cases}. \quad (35)$$

Because $U'^T U' = I_{3N(M-1)}$, we can rewrite the determinant of J_{kink} to be

$$\det J_{\text{kink}} = \det U'^T J_{\text{kink}} U'. \quad (36)$$

The J_{kink} similarity-transformed by U' is written as

$$U'^T J_{\text{kink}} U'[i, j] = \begin{cases} A'_0 \equiv U_0^T H_0 U_0 + 2cI_{3N} & (i = j, 0 \leq i \leq L_0 \text{ or } L_0 + L \leq i \leq 2L_0 + L) \\ -cU_0 & (i = L_0 + 1, j = L_0) \\ -cU_0^T & (i = L_0, j = L_0 + 1) \\ -cU_L^T & (i = L_0 + L - 1, j = L_0 + L) \\ -cU_L & (i = L_0 + L, j = L_0 + L - 1) \\ J_{\text{kink}}[i, j] & (\text{others}) \end{cases}. \quad (37)$$

We have assumed a symmetric transition system that means A_0 and A_L have the same eigenvalues, namely, $A'_0 = A'_L$ in Eq. (37), and we have also used the following relations: $U_0^T U_0 = U_L^T U_L = I_{3N}$. The parts related with equilibrium states in $U'^T J_{\text{kink}} U'$ have a tridiagonal-like band matrix structure. As in Sec. II, the Gaussian elimination method is applied to diagonalize this part. The determinant can be written as follows:

$$\det J_{\text{kink}} = \begin{vmatrix} \bar{B} & O & O \\ O & U'^T J'_{\text{kink}} U' & O \\ O & O & \underline{B} \end{vmatrix}, \quad (38)$$

where $3N(L+1) \times 3N(L+1)$ matrix J'_{kink} is written by

$$J'_{\text{kink}}[k, l] \equiv \begin{cases} U_0 B_{L_0} U_0^T & (k = l = 0) \\ U_L B_{L_0} U_L^T & (k = l = L) \\ A_k & (k = l, 0 < k < L) \\ -cI_{3N} & (k = l \pm 1) \\ O & (\text{others}) \end{cases}, \quad (39)$$

where indices k and l run from 0 to L ; a matrix U'' is a $3N(L+1) \times 3N(L+1)$ square matrix defined by

$$U''[k, l] \equiv \begin{cases} U_0 & (k = l = 0 \text{ or } k = l = L) \\ I_{3N} & (k = l, 0 < k < L) \\ O & (\text{others}) \end{cases}. \quad (40)$$

\bar{B} and \underline{B} are $3NL_0 \times 3NL_0$ diagonal matrices, and these diagonal partial matrices are $\bar{B}[m, m] \equiv B_m$ and $\underline{B}[m, m] \equiv B_{L_0-m}$, respectively. B_m is a $3N \times 3N$ diagonal matrix whose diagonal n th element is denoted to be b_m^n . As in Sec. II, b_m^n is found to obey the following recurrence relation regarding subscript m :

$$b_m^n = \eta_0^n + 2c - c^2 \frac{1}{b_{m-1}^n} \quad (41)$$

with η_0^n being the n th eigenvalue of the Hessian H_0 . The initial value of the recurrence relation is given to be $b_1^n = \eta_0^n + 2c$. We have $3N$ independent recurrence relations according to the index n . In the case of $\eta_0^n \neq 0$, a solution of Eq. (41) is the following, see Eq. (A6):

$$b_m^n = \frac{\alpha_+^n - \alpha_-^n (D_n)^m}{1 - (D_n)^m}, \quad (42)$$

where α_{\pm}^n are defined as

$$\alpha_{\pm}^n \equiv \frac{1}{2} \left(\eta_0^n + 2c \pm \sqrt{(\eta_0^n)^2 + 4c\eta_0^n} \right) \quad (43)$$

with $D_n \equiv \alpha_-^n / \alpha_+^n$. Because D_n is always smaller than 1,

$$b_{\infty}^n = \alpha_+^n. \quad (44)$$

In the case of $\eta_0^n = 0$, n th eigenvalue of the Hessian H_0 is zero, a solution of Eq. (41) is obtained, see Eq. (A11), by

$$b_m^n = c + \frac{c}{m}. \quad (45)$$

The second term in right hand side of Eq. (45) is found to be inversely proportional to m . Because Eq. (42) exponentially decays in m , the value of b_m^n at $\eta_0^n = 0$ converges much slower than that at $\eta_0^n \neq 0$ in larger m . For $m \rightarrow \infty$, Eq. (45) becomes

$$b_{\infty}^n = c. \quad (46)$$

We find Eq. (44) is valid also in the case of $\eta_0^n = 0$, in fact, we can obtain Eq. (46) from Eq. (44) with $\eta_0^n = 0$. We then evaluate the determinant Eq. (38) to be

$$\det J_{\text{kink}} = \det J'_{\text{kink}} \det \bar{B} \det \underline{B} = \det J'_{\text{kink}} \prod_{m=1}^{L_0-1} (\det B_m)^2. \quad (47)$$

We can apply similar operations to non-tunneling case $\det J_0$. The elements of original $3N(M-1) \times 3N(M-1)$ matrix J_0 are given by

$$J_0[i, j] = \begin{cases} A_0 & (i = j) \\ -cI_{3N} & (i = j \pm 1) \\ O & (\text{others}) \end{cases}. \quad (48)$$

We define the following $3N(M-1) \times 3N(M-1)$ matrix U :

$$U[i, j] \equiv \begin{cases} U_0 & (i = j) \\ O & (\text{others}) \end{cases}, \quad (49)$$

where U_0 is the orthogonal matrix to diagonalize H_0 corresponding to an equilibrium state. Using $U^T U = I_{3N(M-1)}$, the determinant of J_0 is transformed into

$$\det J_0 = \det U^T J_0 U = \det J'_0 \prod_{m=1}^{L_0-1} (\det B_m)^2, \quad (50)$$

where

$$J'_0[k, l] \equiv \begin{cases} B_{L_0} & (k = l, k = 0 \text{ or } L) \\ A'_0 & (k = l, 0 < k < L) \\ -cI_{3N} & (k = l \pm 1) \\ O & (\text{others}) \end{cases}. \quad (51)$$

Dividing Eq. (47) by Eq. (50), we obtain the following relation:

$$\frac{\det J_{\text{kink}}}{\det J_0} = \frac{\det J'_{\text{kink}}}{\det J'_0}. \quad (52)$$

Equation (52) indicates that division of determinants for large matrices can be expressed using determinants of smaller matrices. Then, we obtain $L_0 \rightarrow \infty$ limit operating $B_{L_0} \rightarrow B_{\infty}$ in Eqs. (39) and (51). The limit of $L_0 \rightarrow \infty$ corresponds to $\beta \rightarrow \infty$. Namely, we obtain the following equation for

infinite-size full-path matrices, J_{kink} and J_0 , with finite-size local-path matrices, J''_{kink} and J''_0 :

$$\lim_{\beta \rightarrow \infty} \frac{\det J_{\text{kink}}}{\det J_0} = \frac{\det J''_{\text{kink}}}{\det J''_0}, \quad (53)$$

where local path matrices are defined by

$$J''_{\text{kink}}[k, l] \equiv \lim_{L_0 \rightarrow \infty} J'_{\text{kink}}[k, l] = \begin{cases} U_0 B_{\infty} U_0^T & (k = l = 0) \\ U_L B_{\infty} U_L^T & (k = l = L) \\ J'_{\text{kink}}[k, l] & (\text{others}) \end{cases} \quad (54)$$

and

$$J''_0[k, l] \equiv \lim_{L_0 \rightarrow \infty} J'_0[k, l] = \begin{cases} B_{\infty} & (k = l, k = 0 \text{ or } L) \\ J'_0[k, l] & (\text{others}) \end{cases}. \quad (55)$$

Elements of diagonal matrix B_{∞} are given in Eqs. (44) and (46). As in the Sec. II, a zero eigenvalue mode related with the translation of the kink in the imaginary time is handled separately, see Eq. (6). New formula of Φ factor in the infinite β is written as

$$\lim_{\beta \rightarrow \infty} \Phi = \left(\frac{\det J''_{\text{kink}}}{\det J''_0} \right)^{\frac{1}{2}}. \quad (56)$$

Our new formula can be obtained by two elements A_0 and A_L in the Richardson-Althorpe's formula being replaced by $U_0 B_{\infty} U_0^T$. Equation (56) corresponds to Eq. (27) for one-dimensional case. For molecular systems in three-dimensional Cartesian space, however, we must treat the following issues carefully for accurate calculations.

The J''_{kink} is $3N(L+1) \times 3N(L+1)$ matrix corresponding to the Hessian for the isomorphic open polymer consisting of $L+1$ time slices. The extended L_0 equilibrium states only affect the matrix elements associated with the boundary between a pre-extended $L-1$ time slices and extended L_0 time slices. Then, the resulting Hessian J''_{kink} can mathematically be interpreted to be the Hessian of an isomorphic polymer of $L+1$ time slices with a free end boundary condition. This is because B_{∞} has six degenerate eigenvalues of c as shown in Eq. (46), then, $J''_{\text{kink}}[0, 0]$ and $J''_{\text{kink}}[L, L]$ defined in Eq. (54) have associated six degenerate eigenvalues of c , which is equivalent to a Hessian of a "free end" polymer, while the corresponding eigenvalues of $J''_{\text{kink}}[0, 0]$ and $J''_{\text{kink}}[L, L]$ must be $2c$ for the fixed end condition. These six eigenvalues of c arise from translations and rotations of a molecule in an equilibrium state. The free end boundary condition of the isomorphic polymer produces six zero eigenvalue modes related with "translation" and "rotation" of the whole polymer. The J''_0 is also in the same condition. The factors associated with these zero eigenvalue modes appeared in both numerator and denominator of Eq. (56). In Sec. III B, we derive the limiting expression of the ratio regarding the vanishing eigenvalues at the infinite β .

It is worthwhile to note that the above free end boundary condition always appears irrespective of the boundary condition applied to the polymer of $2L_0 + L - 1$ time slices, which is evident from Eqs. (44) and (46) for the case of $L_0 \rightarrow \infty$.

B. Zero eigenvalue modes for translations and rotations

We first extract terms related with the zero eigenvalues of translations and rotations of the isomorphic open polymer from the fluctuation determinant factor Φ for the infinite β in molecular systems. We denote orthonormal eigenvectors for these zero eigenvalues as v_r^z ($r = 1, 2, \dots, 6$) and ($z = 0$ or kink) for J''_{kink} and J''_0 , respectively. The corresponding $3N(L+1) \times 6$ eigenvector matrix v_z for $z = 0$ or kink is defined to be $v_z \equiv (v_1^z, v_2^z, \dots, v_6^z)$. Using these matrices, Eq. (53) is rewritten as

$$\frac{\det J''_{\text{kink}}}{\det J''_0} = \frac{\widetilde{\det} J''_{\text{kink}}}{\widetilde{\det} J''_0} \frac{\det v_{\text{kink}}^T J''_{\text{kink}} v_{\text{kink}}}{\det v_0^T J''_0 v_0}, \quad (57)$$

where $\widetilde{\det}$ indicates a determinant without zero eigenvalue modes for translations and rotations. Here, we introduce u_{kr}^z that constitutes orthonormal vectors describing translations and rotations of the system for a time slice k ($0 \leq k \leq L$), the subscript r specifies the associated mode, $r = 1, \dots, 6$, and $z = 0$ or kink. The size of the vector u_{kr}^z is $3N(L+1)$. A procedure to generate a set of u_{kr}^z is described in Appendix B. We define the following matrix μ_z using u_{kr}^z :

$$\mu_z \equiv (u_{01}^z, u_{02}^z, \dots, u_{06}^z, u_{11}^z, \dots, u_{kr}^z, \dots, u_{L6}^z). \quad (58)$$

Then, we express a zero mode eigenvector matrix v_z using μ_z as

$$v_z = \mu_z \tilde{u}_z. \quad (59)$$

To clarify the meaning of \tilde{u}_z , we rewrite the relation $v_z^T J''_z v_z = O$ to be

$$v_z^T J''_z v_z = \tilde{u}_z^T j_z \tilde{u}_z = O, \quad (60)$$

where $j_z \equiv \mu_z^T J''_z \mu_z$, that is, a $6(L+1) \times 6(L+1)$ matrix. Then, the \tilde{u}_z is found to be an eigenvector matrix of j_z for translations and rotations. We denote the elements of \tilde{u}_z as $\alpha_{kr'r}^z \equiv \tilde{u}_z[6k+r', r]$ for later use. Using this notation, the eigenvector v_r^z is written as $v_r^z = \sum_{k=0}^L \sum_{r'=1}^6 \alpha_{kr'r}^z u_{kr'r}^z$. Because $v_z^T v_z = I_6$ and $\mu_z^T \mu_z = I_{6(L+1)}$, $\tilde{u}_z^T \tilde{u}_z = I_6$, namely, $(\tilde{u}_z^T \tilde{u}_z)[r, r] = \sum_{k=0}^L \sum_{r'=1}^6 |\alpha_{kr'r}^z|^2 = 1$. In the case of $z = 0$, the factor $\sum_{r'=1}^6 |\alpha_{kr'r}^0|^2$ is equal for all imaginary time slices k . Therefore, we obtain a relation of $\sum_{r'=1}^6 |\alpha_{kr'r}^0|^2 = 1/(L+1)$ for any k and r . Here, we define $j'_z \equiv \mu_z^T J'_z \mu_z$ that is a finite L_0 version of $j_z = \lim_{L_0 \rightarrow \infty} \mu_z^T J'_z \mu_z$ for the following formulation. In the case of $z = 0$, the elements of j'_0 is written as

$$j'_0[k, l] = \begin{cases} xI_6 & (k = l, k = 0 \text{ or } L) \\ 2cI_6 & (k = l, 0 < k < L) \\ -cI_6 & (k = \pm l) \\ 0 & (\text{others}) \end{cases}, \quad (61)$$

where $\lim_{L_0 \rightarrow \infty} x = c$, see Eq. (46). In this case, the elements of \tilde{u}_z have a relation of $\sum_{r'=1}^6 |\alpha_{kr'r}^0|^2 = 1/(L+1)$ and then,

$$\tilde{u}_0[k] = \left(\frac{1}{\sqrt{L+1}} \right)^6 \bar{I}_6, \quad (62)$$

where \bar{I}_6 indicates a 6×6 rotation matrix. Using Eqs. (61) and (62), we obtain the following relation:

$$\begin{aligned} \det v_0^T J''_0 v_0 &= \det \tilde{u}_0^T j_0 \tilde{u}_0 = \lim_{x \rightarrow c} \det \tilde{u}_0^T j'_0 \tilde{u}_0 \\ &= \lim_{x \rightarrow c} \left(2(x-c) \frac{1}{L+1} \right)^6. \end{aligned} \quad (63)$$

On the other hand, in the case of $z = \text{kink}$, we can obtain \tilde{u}_{kink} by numerically diagonalizing the matrix j_{kink} . For the following discussion, we consider j'_{kink} for a given L . We further assume the following relation without loss of generality: $A_1 = A_0$ and $A_{L-1} = A_L$; due to this assumption, the eigenvectors of j_{kink} have relations of the elements $\sum_{r'=1}^6 |\alpha_{0r'r}^{\text{kink}}|^2 = \sum_{r'=1}^6 |\alpha_{1r'r}^{\text{kink}}|^2 = \sum_{r'=1}^6 |\alpha_{Lr'r}^{\text{kink}}|^2 = \sum_{r'=1}^6 |\alpha_{L+1,r'r}^{\text{kink}}|^2$. We rewrite these elements as $1/(L_r+1) \equiv \sum_{r'=1}^6 |\alpha_{0r'r}^{\text{kink}}|^2$ to facilitate the formal similarity with $\sum_{r'=1}^6 |\alpha_{kr'r}^0|^2 = 1/(L+1)$. The elements of j'_{kink} become

$$j'_{\text{kink}}[k, l] = \begin{cases} xI_6 & (k = l, k = 0 \text{ or } L) \\ 2cI_6 & (k = l, k = 1 \text{ or } L-1) \\ -cI_6 & (k = \pm l, k + l = 1 \text{ or } 2L-1) \\ O & (\text{other than tridiagonal}) \\ \text{various} & (\text{others}) \end{cases}. \quad (64)$$

Using Eq. (64), the diagonal elements of $\tilde{u}_{\text{kink}}^T j'_{\text{kink}} \tilde{u}_{\text{kink}}$ are written as

$$\tilde{u}_{\text{kink}}^T j'_{\text{kink}} \tilde{u}_{\text{kink}}[r, r] = 2(x-c) \frac{1}{L_r+1} + \Theta_r. \quad (65)$$

In the case of $z = 0$, the quantity Θ_r is zero from Eqs. (61) and (62). On the other hand, for $z = \text{kink}$, since Θ_r is independent of x and Eq. (65) is zero for limit of $x \rightarrow c$, we immediately obtain $\Theta_r = 0$. We then obtain

$$\begin{aligned} \det v_{\text{kink}}^T J''_{\text{kink}} v_{\text{kink}} &= \det \tilde{u}_{\text{kink}}^T j_{\text{kink}} \tilde{u}_{\text{kink}} \\ &= \lim_{x \rightarrow c} \det \tilde{u}_{\text{kink}}^T j'_{\text{kink}} \tilde{u}_{\text{kink}} \\ &= \lim_{x \rightarrow c} \prod_{r=1}^6 2(x-c) \frac{1}{L_r+1}. \end{aligned} \quad (66)$$

Substituting Eqs. (63) and (66) into Eq. (57), we reach the following relation:

$$\frac{\det J''_{\text{kink}}}{\det J''_0} = \frac{\widetilde{\det} J''_{\text{kink}}}{\widetilde{\det} J''_0} \prod_{r=1}^6 \frac{L+1}{L_r+1}. \quad (67)$$

Finally, we obtain our new formula for the Φ factor as

$$\lim_{\beta \rightarrow \infty} \Phi = \left(\frac{\widetilde{\det}' J''_{\text{kink}}}{\widetilde{\det} J''_0} \prod_{r=1}^6 \frac{L+1}{L_r+1} \right)^{\frac{1}{2}}, \quad (68)$$

where the prime symbol in $\widetilde{\det}'$ indicates a determinant without a zero eigenvalue mode associated with the translation of the kink in the imaginary time as in the previous discussion.

C. Numerical application to HO₂

1. Computational details

In this subsection, we present an application of our new formula, Eq. (68), to a molecular system. We have adopted a hydrogen transfer in HO₂ molecule as a model system. The system is described by a double many-body expansion (DMBE) IV potential⁵⁵ to compare our results with previous study.⁴¹ As in Sec. II, we use the parameter $\beta_L \equiv L\Delta\tau/\hbar$ to specify the imaginary time duration for our calculations. Then, we employed the following parameters, $\beta_L\hbar = 5000$ a.u. and $L = 128$. As in Sec. II, we used L-BFGS subroutine^{53,54} for optimizing the isomorphic open polymers to find the stationary path, and LAPACK library for the diagonalization of matrices; in the course of the calculations, we have optimized whole polymer coordinates including $q^{(0)}$ and $q^{(M)}$ to find the single kink path.

Here, we summarize a recipe to calculate L_r :

1. Create a μ_{kink} matrix for all translations and rotations using the method described in Appendix B. Here, the size of matrix becomes $3N(L+1) \times 6(L+1)$.
2. Calculate $j_{\text{kink}} = \mu_{\text{kink}}^T J''_{\text{kink}} \mu_{\text{kink}}$.
3. Diagonalize j_{kink} and obtain \tilde{u}_{kink} .
4. Calculate L_r from $L_r + 1 = 1/\sum_{r'=1}^6 |\alpha_{0r'}^{\text{kink}}|^2$ for all r .

2. Evaluation of tunneling splitting

We first show the numerical tunneling splitting as a function of β_L . The results obtained by our new formula (68) are presented together with the results by the Richardson-Althorpe's formula in Fig. 2. Computational results for $\beta_L\hbar = 5000, 10000, 15000, 20000, 40000, 60000, 80000, 120000,$ and 160000 a.u. are shown with fixed $\Delta\tau = (5000/128)$ a.u. In the Richardson-Althorpe's formula, which we call finite β form, the value of the tunneling splitting clearly depends on the value of β in the time range presented; the error of the tunneling splitting slowly decreases with β . The slow decay is caused by the polynomial decay of term in Eq. (45). On

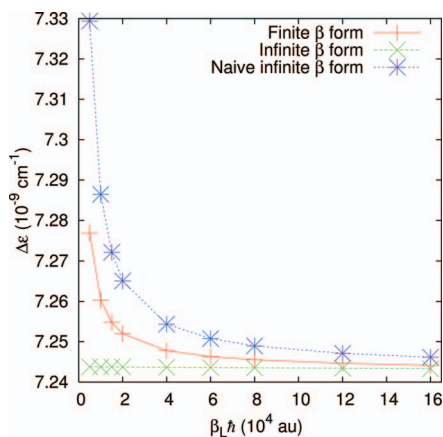


FIG. 2. Tunneling splittings calculated by the Richardson-Althorpe's form (finite β form) and new form (infinite β form) for HO₂ intra-molecular hydrogen transfer are plotted for various $\beta\hbar$. The computed results by the naive infinite β form, which is defined by $\Phi = \sqrt{\det' J''_{\text{kink}}/\det J''_0}$, are plotted for comparison.

the other hand, we numerically confirmed that the new formula, which we call infinite β form, is independent of β_L and the graph is found to be almost flat in the figure. The finite β form, which is the Richardson-Althorpe's formula, needs about 4 times longer imaginary time duration to obtain the converged value whose error is less than 1.0×10^{-11} cm⁻¹. In addition, we introduce another approximate formula where the factor associated with L_r in Eq. (67) is set to be unity: $\prod_{r=1}^6 (L + 1/L_r + 1) = 1$, which means that contributions from the zero eigenvalues are assumed to be identical both for J''_{kink} and J''_0 . We call it a naive infinite β form. The β_L dependence of the tunneling splitting is found to be even worse than the result by the finite β form. This indicates the importance of the careful treatment of zero eigenvalues presented, for example, in Eq. (57).

Here, we examine β_L dependence of $\prod_{r=1}^6 (L + 1/L_r + 1)$ factor. We first define an index l_{sum} by

$$l_{\text{sum}} \equiv \sum_{r=1}^6 l_r, \quad (69)$$

where $l_r \equiv L - L_r$. The above factor is approximated, with assumption $|l_r| \ll L + 1$, as

$$\prod_{r=1}^6 \frac{L+1}{L_r+1} = \frac{L+1}{L+1-l_{\text{sum}} + O(l_r l_{r'}/(L+1))} \approx 1 + \frac{l_{\text{sum}}}{L}. \quad (70)$$

For a given L , the above factor is found to depend on only single parameter l_{sum} . In the results presented in Fig. 2, the value of l_{sum} is calculated to be about 3 for all β_L , which indicates l_{sum} does not depend on β_L for a given $\Delta\tau$. Then, we examine $\Delta\tau$ dependence of l_{sum} ; we plotted l_{sum} using various $1/\Delta\tau$, which is presented in Fig. 3. All computed results are found to stay on a single line very well, and we obtain a constant $\Delta\tau l_{\text{sum}}$ for any $\Delta\tau$ presented in the figure. The value of $\Delta\tau l_{\text{sum}}$ is calculated to be 117.7 a.u. in a least square fitting calculation for this system. Then, Eq. (70) is written as

$$\prod_{r=1}^6 \frac{L+1}{L_r+1} \approx 1 + \frac{l_{\text{sum}} \Delta\tau}{\beta_L \hbar}. \quad (71)$$

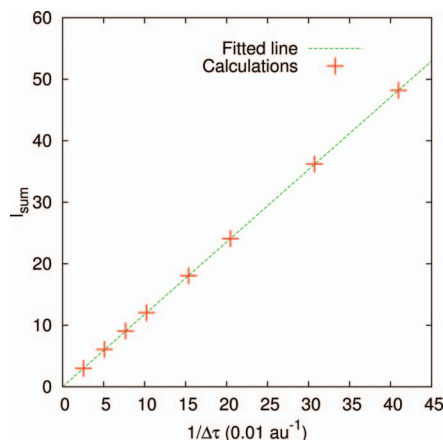


FIG. 3. The quantity l_{sum} is plotted as a function of $\Delta\tau$. The line is obtained by a least square fitting of presented data.

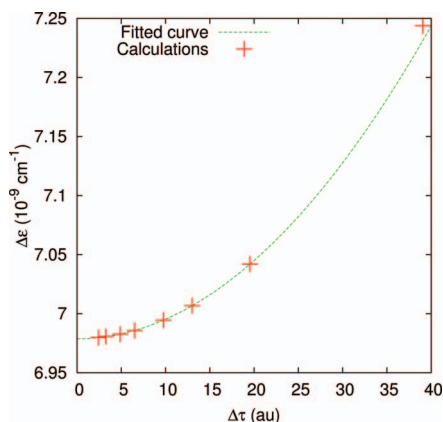


FIG. 4. Computed tunneling splittings for HO₂ hydrogen transfer as a function of $\Delta\tau$. Curve is obtained by a least square fitting for the data $\Delta\tau < 20.7$ a.u.

Since the quantity $\Delta\tau l_{\text{sum}}$ has been found to be a constant, the above factor converges on a limiting value by β_L^{-1} ; this is consistent with the slowly converging behavior observed in Fig. 2 for the naive infinite β form. We have also found that the Richardson-Althorpe's finite β form has a slowly decaying term as shown in Eq. (45). The full infinite β form of Eq. (68) is free from these slowly decaying behaviors, which must be useful to reduce the number of imaginary time slices in numerical calculations.

As in Sec. II C, we computed tunneling splittings for various $\Delta\tau$, which are plotted in Fig. 4, and the calculated values are fitted using Eq. (33). We show the results with $\beta_L \hbar = 5000$ a.u. and $L = 128, 256, 384, 512, 768, 1024, 1537,$ and 2048 in Fig. 4. Where the $\Delta\tau$ is small, all plots are found to stay on a parabola of the fitted curve. The extrapolated value is calculated to be $\Delta\varepsilon_{\text{true}} = 6.98 \times 10^{-9} \text{ cm}^{-1}$, which is in good agreement with the Richardson-Althorpe's result. It is noted that we have used calculated tunneling splittings for $\Delta\tau \leq 20.7$ for the least square fitting with Eq. (33); these calculated values are selected so as to be in the range of 1% error compared with $\Delta\varepsilon_{\text{true}}$.

3. On the numerical accuracy of Hessian matrix

In the above calculations, we have applied the following Hessian purification technique to avoid the accumulation of numerical errors due to repeated use of the same numerical Hessian matrix for evaluating Eq. (9). Especially, when the zero eigenvalue is numerically non-zero, the error significantly affects the final computational result. Here, we present a recipe to remedy the errors, which decouples the translations and rotations from computed Hessians.⁵⁶ The purification process is summarized as follows:

1. Diagonalize the Hessian H_0 for an equilibrium state and obtain its eigenvalues $\{\eta_0^n\}$ and eigenvector matrix U_0 .
2. Replace eigenvalues concerning the translations and rotations to exactly zero, and create a diagonal matrix \bar{H}_0 whose components are eigenvalues η_0^n .
3. Calculate purified Hessian, $H_0^{\text{purify}} = U_0 \bar{H}_0 U_0^T$.

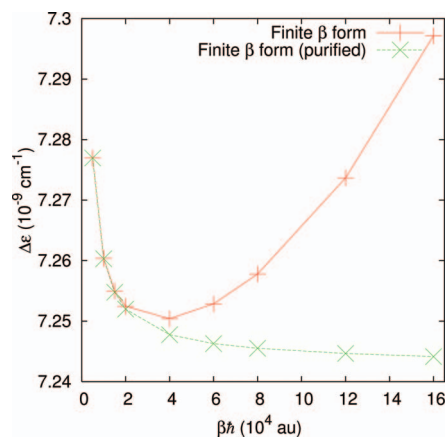


FIG. 5. Tunneling splittings calculated by the Richardson-Althorpe's form. The symbol "x" indicates the results with the Hessian purification and the symbol "+" without the Hessian purification. All the calculations have been performed using the same $\Delta\tau = 5000/128$ a.u.

4. Repeat the same procedure for Hessian H_L for the other equilibrium state.

To demonstrate the importance of the Hessian purification, we present the calculated tunneling splitting by the Richardson-Althorpe's formula with and without the purification. As shown in Fig. 5, computed results show an artificial turnover with β , which is caused by the accumulated numerical errors, when the purification is not applied. The purification is found to exclude the artifact; the computed value approaches to a certain value when the β increases. We have applied the Hessian purification to extra H_0 when we extend β by adding the local states to the ends of the isomorphic polymer, and to all H_0 in J_0 to decrease computational errors, because the same local state is repeated in whole polymer for J_0 calculation.

IV. COMBINATION WITH THE *AB INITIO* MOLECULAR ORBITAL THEORY

A. Computational details

Here, we describe the details of our calculations combined with the *ab initio* molecular orbital theory. We have developed our original code for main part of the path integral instanton calculations, which is written by C language. For diagonalizing matrices, we use LAPACK library.⁵⁷ To optimize the structure of isomorphic open chain polymer, L-BFGS-B subroutine^{53,54} is used. Electronic structure for each time slice is determined by the *ab initio* molecular orbital calculation. The electronic structure and associated potential, forces, and Hessians are calculated by calling GAMESS quantum chemical program⁵⁸ on the fly where output functions are modified for our purpose. The program is parallelized by MPI protocol and each process calculates energies, forces, or Hessian of single imaginary time slice independently. The strategy could work in combination with the parallelization of GAMESS program, although we have not used it for the present calculation except program tests, because the current system is too small for parallel calculation in the quantum chemistry.

Standalone quantum chemical calculations to discuss molecular structures and the normal modes in Sec. IV B are done using the normal GAMESS program.

B. Computational results

In this subsection, we apply several quantum chemical methods for the interatomic force field to examine how the difference of basis functions and electronic correlations affects the computational results of tunneling splittings. We first checked equilibrium structure of an ammonia molecule and the reaction barrier of the umbrella flip motion using various quantum chemical methods. We then applied our *ab initio* discretized path integral instanton method to the ammonia molecule and calculated the tunneling splittings for the umbrella flips.

1. Molecular structure of ammonia

For representing the structure of an ammonia molecule using molecular orbital theory, the extended basis function is required with enough number of polarization functions for describing its lone-pair orbital. To obtain an accurate potential barrier of the ammonia umbrella flips, electronic correlation should also be included in the electronic Hamiltonian. Considering these requirements, we tested various basis functions for restricted Hartree-Fock (RHF) theory⁵⁹ with the second order Møller–Plesset perturbation theory (MP2).⁶⁰ We then selected three candidates of basis functions, 6-311++G(3d3p),^{61–64} 6-31++G(2d2p),^{62–66} and ktzvpp (Karlsruhe valence triple zeta basis with a set of double polarization bases).^{67,68} The equilibrium structure of the ammonia molecule is shown in Table I. In these basis functions, the structure using 6-311++G(3d3p) shows the best agreement with the experimental data, and the 6-31++G(2d2p) and ktzvpp, respectively, overestimates and underestimates the N-H bond lengths and also H-N-H angles. We also show the N-H bond length at a transition state of the umbrella flip motion and the associated reaction barrier for each basis function. The reaction barrier becomes higher in order of the 6-311++G(3d3p), 6-31++G(2d2p), and ktzvpp. We note that these values of barrier heights do not include the zero point energy. On the other hand, when we optimize the ammonia structure using standard RHF⁵⁹ calculation, the structure of the equilibrium state becomes slightly different from the experimental data, however, for later comparisons,

TABLE I. Dependences of computational methods for ammonia structures.

	N-H (GS) (Å)	H-N-H (GS) (degree)	N-H (TS) (Å)	Barrier (kcal/mol)
MP2/6-311++G(3d,3p)	1.0116	106.78	0.9955	5.241
MP2/6-31++G(2d,2p)	1.0123	106.79	0.9965	5.284
MP2/ktzvpp	1.0110	106.60	0.9945	5.365
RHF/6-311++G(3d,3p)	0.9990	107.61	0.9851	5.319
RHF/6-31++G(2d,2p)	0.9996	107.85	0.9859	5.124
Experiment ^a	1.0116	106.68		

^aValues are obtained from Refs. 46 and 70.

we also chose two basis functions which give the similar reaction barriers with RHF to above three basis functions for RHF-MP2, the 6-311++G(3d3p), and 6-31++G(2d2p). We show the computed structures and barrier heights for these RHF calculations below the list of RHF-MP2 results in Table I. Without the electronic correlation, H-N-H angles of the equilibrium state become about one degree larger than with the correlation function (or experimental data), and the N-H bond lengths become slightly shorter. These differences affect to the molecular vibrations as follows. In the case of 6-311++G(3d3p) basis function, the frequencies of the normal modes for RHF are calculated larger than RHF-MP2 results for both potential minimum and saddle structures, for example, a frequency of the inversion mode in the equilibrium state is calculated as 1057 and 1129 cm^{-1} , respectively, whose experimental value is 950 cm^{-1} .⁶⁹ We note that these computed normal mode frequencies do not include the quantum effect of fluctuating protons. The differences of the zero point energy in the harmonic normal mode approximation for the saddle state from the equilibrium state are -0.8583 and -1.0830 kcal/mol for RHF-MP2 and RHF, respectively, and then the total barrier height of 4.383 and 4.236 kcal/mol are not much different.

In Subsection IV B 2, we examine these five quantum chemical methods to combine with our method for calculating the tunneling splittings of the ammonia umbrella flips.

2. Evaluation of tunneling splitting for NH₃

We show computational results of the tunneling splittings for the ammonia umbrella flip of NH₃ using five different quantum chemical methods for the force fields of interatomic potential in Table II. Best result compared with the experimental data is given by the RHF-MP2/6-311++G(3d3p) which presents the closest equilibrium structure to the experimental structure among five calculations; the error is found to be less than 1%. For the RHF-MP2/6-31++G(2d2p) result, the tunneling splitting is slightly overestimated. In Fig. 6, we present $\Delta\tau$ dependent tunneling splittings and other quantities. In each least square fitting, we ignored a plotted result of largest $\Delta\tau$ due to our empirical threshold of $C\Delta\tau / \Delta\varepsilon < 0.01$ for this system. This threshold is self-consistently tested. An example of computed tunneling splittings $\Delta\varepsilon(\Delta\tau)$ for NH₃ umbrella flips with RHF-MP2/6-311++G(3d3p) results, and a fitted curve is drawn in

TABLE II. Dependences of computational methods for tunneling splittings of ammonia flips.

	S_{kink} (a.u.)	Φ	$\Delta\varepsilon$ (cm^{-1})
MP2/6-311++G(3d,3p)	8.323	155.90	0.787
MP2/6-31++G(2d,2p)	8.381	142.77	0.814
MP2/ktzvpp	8.470	152.70	0.700
RHF/6-311++G(3d,3p)	8.023	120.85	1.346
RHF/6-31++G(2d,2p)	7.786	124.27	1.634
Experiment ^a			0.793

^aValues are obtained from Refs. 46 and 47.

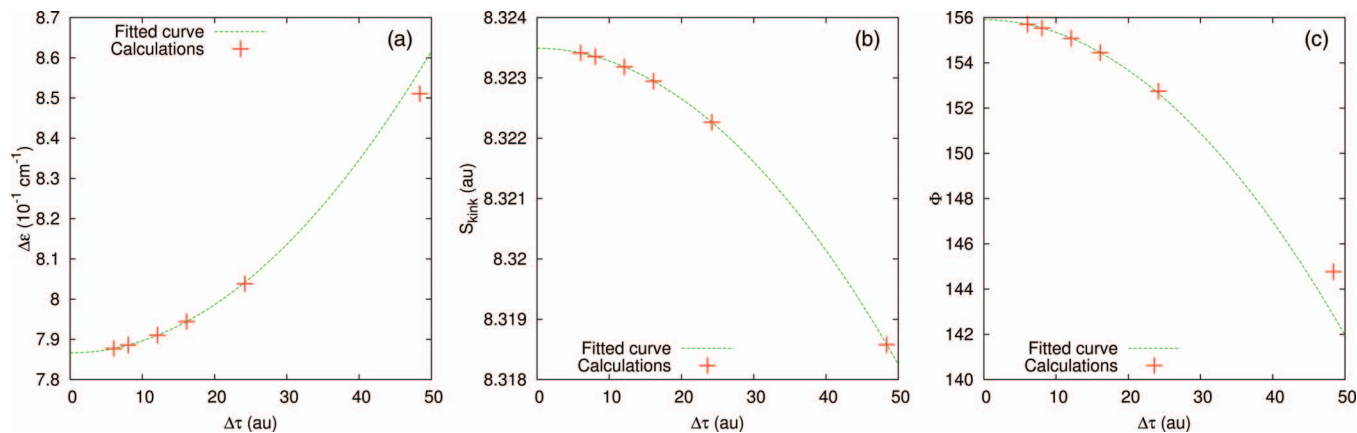


FIG. 6. The imaginary time step $\Delta\tau$ dependences of (a) $\Delta\epsilon$, (b) S_{kink} , and (c) Φ for NH_3 umbrella flips. Solid curves are least square fitted using four points of smaller $\Delta\tau$, respectively.

Fig. 6(a). Results in Fig. 6 are used parameters; $\beta_L \hbar = 6000$ a.u. and $L = 124, 248, 372, 496, 744,$ and 992 . We can read that the approximation of Eq. (33) works very well from the figure. For comparison, we calculated the tunneling splitting for both Richardson-Althorpe's method and our method with parameters; $\beta_L \hbar = 6000$ a.u. and $L = 300$. The results of the Richardson-Althorpe's method and our method are 0.768 and 0.798 cm^{-1} with the same $S_{\text{kink}} = 8.323$ a.u. The Φ factor is 153.71 and 159.79 , respectively. The difference is caused by the effect of $\beta \rightarrow \infty$ limit and when the parameters are extended to $\beta_L \hbar = 10000$ a.u. and $L = 500$, the tunneling splitting by the Richardson-Althorpe's method is calculated as 0.796 cm^{-1} . Our method presents a result in an equal quality of Richardson-Althorpe's method with $L = 500$ imaginary time slices using only $L = 300$ in this case; our method significantly reduces the computational cost to achieve the same numerical accuracy by the Richardson-Althorpe's method.

We also used the same strategy to obtain $\Delta\tau \rightarrow 0$ limit for other similar properties as the single kink action S_{kink} and Φ factor because these are also approximated as

$$S_{\text{kink}}(\Delta\tau) \approx S_{\text{kink}}(0) + C_S \Delta\tau^2 \quad (72)$$

and

$$\Phi(\Delta\tau) \approx \Phi(0) + C_\Phi \Delta\tau^2, \quad (73)$$

where C_S and C_Φ are constants. We re-define these values as $S_{\text{kink}} \equiv S_{\text{kink}}(0)$ and $\Phi \equiv \Phi(0)$ in $\Delta\tau \rightarrow 0$ limit. Examples of computed $S_{\text{kink}}(\Delta\tau)$ and $\Phi(\Delta\tau)$ for NH_3 umbrella flips, and these fitted curves are shown in Figs. 6(b) and 6(c), respectively. We used the same data points of $\Delta\epsilon$ for these fitting instead of determining a threshold for each property. Approximations in Eqs. (72) and (73) work as well as Eq. (33) in Fig. 6. Compared with the result of the RHF-MP2/6-311++G(3d3p), the Φ factor is relatively small, which indicates the contributions from the harmonic fluctuations along the single kink path; the curvature of computed potential surface along the single kink path is slightly less accurate than RHF-MP2/6-311++G(3d3p). The computed result of RHF-MP2/ktzvpv is about 12% underestimated because the reaction barrier is underestimated, and then S_{kink} becomes large. On the other hand, for both RHF calcula-

tions, the computed tunneling splittings are approximately two times overestimated than the experimental value, because both the S_{kink} values and Φ factors are calculated smaller than RHF-MP2 results. Comparing RHF/6-311++G(3d3p) result with RHF-MP2/6-311++G(3d3p), the factor associated with S_{kink} is about 1.32 times larger and Φ^{-1} factor is 1.3 times larger, then, total tunneling splitting $\Delta\epsilon$ is 1.71 times larger. The value of S_{kink} for RHF/6-311++G(3d3p) becomes smaller than RHF-MP2/6-311++G(3d3p) because the H-N-H angle of equilibrium states for RHF calculation is larger than with RHF-MP2, and distances which atoms travel between two equilibrium states become shorter during an umbrella flip because the angle of H-N-H is larger than RHF-MP2 in equilibrium structure, see Table I. The Φ factor is associated with the curvature of the potential surface for the system at the imaginary time slices; see the difference of the normal modes between RHF and RHF-MP2 discussed in Sec. IV B 1. From these examinations, we have to carefully select the quantum chemical method for interatomic force field when calculating the tunneling splitting using the *ab initio* discretized path integral instanton method. The quantum chemical method must enough accurately represent all of the equilibrium structure, reaction barrier, and curvature of the potential surface along the single kink path.

We have calculated Hessians for all the imaginary time slices $L + 1$. In this case, our new algorithm enables us to reduce the computational cost by decreasing the size of isomorphic polymer without deteriorating numerical accuracy. However, in another strategy, the computational cost can be significantly saved by interpolating the Hessian components between *ab initio* calculations on the tunneling path, such as Mil'nikov and Nakamura's method.³⁵⁻³⁷ We could also apply such method to interpolate the Hessians for imaginary time slices using the limited number of *ab initio* calculations on the tunneling path.

V. CONCLUSIONS

To accurately evaluate tunneling splittings, we need to take the zero temperature limit, or the limit of long imaginary time duration. In the Richardson-Althorpe's formula, the

duration is adopted to be long enough for required accuracy. In the present paper, however, a slowly decaying term with respect to the imaginary time is found to be contained in the formula. Thus, we need long imaginary time duration for accurate calculations, which makes the computational cost more expensive and causes an accumulation of numerical Hessian errors. In the present study, we develop a new formula to alleviate the above-mentioned situation. We derived the formula for the infinite imaginary time limit which is taken analytically. The resulting formula corresponds to be a path for a finite time duration that minimizes an imaginary time action with a free boundary condition. Then, we can calculate tunneling splittings for the infinite time limit using the path in the finite time duration. Reducing the number of imaginary time slices, we significantly save the computational cost and additionally improve the accuracy of the calculation avoiding the accumulated numerical Hessian errors. We also find another problem for molecular systems in three-dimensional space. The ratio of vanishing terms in the infinite time limit appears in the expression of the tunneling splitting. The problematic terms are analytically handled to avoid numerical errors. We have successfully applied our formula to model systems and demonstrated the efficiency of the method.

Our formula enables us to analytically take the infinite time limit and reduces the computational cost due to reduction of the imaginary time duration considered. This advantage is important to develop a hybrid method of our formula with *ab initio* molecular orbital calculations. This type method enables us to improve the quality of the potential energy surface systematically. We demonstrated the hybrid method to calculate tunneling splittings for the ground state of the ammonia umbrella flips. We first investigated the selection of the quantum chemical force field for accurate numerical calculations. Then, the results of our calculation are found to be in excellent agreement with experimental measurements. The results presented in this paper indicate that our method works very well when we select the appropriate interatomic quantum chemical force field.

ACKNOWLEDGMENTS

This work was partially supported by the Grant-in-Aid for Scientific Research (C) (Grant No. 23550011) from the Japan Society for the Promotion of Science (JSPS) and by the Strategic Programs for Innovative Research (SPIRE), MEXT, and the Computational Materials Science Initiative (CMSI), Japan. A portion of the computations was performed at the Research Center for Computational Science, Okazaki, Japan.

APPENDIX A: A SOLUTION OF THE RECURRENCE EQS. (14) AND (41)

In this Appendix A, we note a way how to obtain solution for b_m . The recurrence relation of b_m is written by

$$b_m = \eta_0 + 2c - c^2 \frac{1}{b_{m-1}}. \quad (\text{A1})$$

Here, we consider two cases, $\eta_0 \neq 0$ and $\eta_0 = 0$.

First, in the case of $\eta_0 \neq 0$, the following two relations are obtained from Eq. (A1):

$$b_m - \alpha_{\pm} = \frac{(\eta_0 + 2c - \alpha_{\pm})(b_{m-1} - \alpha_{\pm})}{b_{m-1}}, \quad (\text{A2})$$

where

$$\alpha_{\pm} \equiv \frac{1}{2}(\eta_0 + 2c \pm \sqrt{(\eta_0 + 2c)^2 - 4c^2}). \quad (\text{A3})$$

We divide two equations in Eq. (A2) and define f_m as

$$\begin{aligned} f_m &\equiv \frac{(b_m - \alpha_+)}{(b_m - \alpha_-)} = \frac{(\eta_0 + 2c - \alpha_+)(b_{m-1} - \alpha_+)}{(\eta_0 + 2c - \alpha_-)(b_{m-1} - \alpha_-)} \\ &= \frac{\alpha_-}{\alpha_+} f_{m-1} \equiv D f_{m-1}. \end{aligned} \quad (\text{A4})$$

The f_m is a geometric series and the solution is readily obtained by

$$f_m = f_1 D^{m-1}. \quad (\text{A5})$$

Returning to b_m , we obtain

$$b_m = \frac{\alpha_+ - \alpha_- f_1 D^{m-1}}{1 - f_1 D^{m-1}}. \quad (\text{A6})$$

Next, in the case of $\eta_0 = 0$, the following relation is obtained from Eq. (A1):

$$b_m - c = \frac{c(b_{m-1} - c)}{b_{m-1}}. \quad (\text{A7})$$

Defining d_m , Eq. (A7) is rewritten as

$$d_m \equiv b_m - c = \frac{c d_{m-1}}{d_{m-1} + c}. \quad (\text{A8})$$

An inverse of Eq. (A8) is taken:

$$e_m \equiv \frac{1}{d_m} = e_{m-1} + \frac{1}{c}. \quad (\text{A9})$$

The e_m is an arithmetical series and the solution is obtained by

$$e_m = e_1 + (m-1) \frac{1}{c}. \quad (\text{A10})$$

Returning to b_m , we obtain

$$b_m = c + \frac{c}{c e_1 + (m-1)}. \quad (\text{A11})$$

APPENDIX B: ORTHONORMAL VECTORS FOR TRANSLATIONS AND ROTATIONS

In this appendix, we note a way to make a set of orthonormal translation and rotation vectors for a molecular system of each imaginary time slice k . In the first step, we prepare non-orthogonal vectors. Three translation vectors are written by

1. A translation vector to x -direction u'_1 :
 $q_{3i-2} = 1/\sqrt{N}$, $q_{3i-1} = q_{3i} = 0$, ($i = 1, \dots, N$),
2. A translation vector to y -direction u'_2 :
 $q_{3i-1} = 1/\sqrt{N}$, $q_{3i} = q_{3i-2} = 0$, ($i = 1, \dots, N$),
3. A translation vector to z -direction u'_3 :
 $q_{3i} = 1/\sqrt{N}$, $q_{3i-2} = q_{3i-1} = 0$, ($i = 1, \dots, N$),

where N is the number of atoms in the system. The q_n indicates n th element of corresponding vector. On the other hand, three rotation vectors are written by

1. A rotation vector around z -axis u'_4 :

$$q_{3i-2} = -C_z y_i, q_{3i-1} = C_z x_i, q_{3i} = 0, (i = 1, \dots, N),$$
2. A rotation vector around x -axis u'_5 :

$$q_{3i-2} = 0, q_{3i-1} = -C_x z_i, q_{3i} = C_x y_i, (i = 1, \dots, N),$$
3. A rotation vector around y -axis u'_6 :

$$q_{3i-2} = C_y z_i, q_{3i-1} = 0, q_{3i} = -C_y x_i, (i = 1, \dots, N),$$

where C_s ($s = x, y, z$) are constants and $x_i, y_i,$ and z_i denote coordinates of i th atom. To obtain orthogonal vectors, we diagonalize the following 6×6 matrix Q with elements $Q_{ij} \equiv u_i^T u'_j$ and obtain its eigenvector matrix u'' . Using the elements of the eigenvector matrix $u''_{r'}$, an orthogonal vector for these translations and rotations is written as $u_r = \sum_{r'=1}^6 u''_{r'} u'_{r'}$ ($r = 1, 2, \dots, 6$). Normalizing these vectors, we obtain a set of orthonormal vectors for translations and rotations. Then, we put these u_r into the corresponding part of u_{kr}^z , while other elements of u_{kr}^z are set to be zero.

¹H. Nakamura and G. Mil'nikov, *Quantum Mechanical Tunneling in Chemical Physics* (CRC Press, Boca Raton, 2014).
²D. DeVault, *Quantum-Mechanical Tunnelling in Biological Systems* (Cambridge University Press, Melbourne, 1981).
³T. Kawatsu, *Pept. Sci.* **100**, 100 (2013).
⁴S. Coleman, *Aspects of Symmetry* (Cambridge University Press, New York, 1985).
⁵A. Altland and B. Simons, *Condensed Matter Field Theory* (Cambridge University Press, New York, 2006).
⁶D. M. Ceperley and G. Jacucci, *Phys. Rev. Lett.* **58**, 1648 (1987).
⁷A. Kuki and P. G. Wolynes, *Science* **236**, 1647 (1987).
⁸C. Alexandrou and J. W. Negele, *Phys. Rev. C* **37**, 1513 (1988).
⁹M. Marchi and D. Chandler, *J. Chem. Phys.* **95**, 889 (1991).
¹⁰D. F. Coker and R. O. Watts, *J. Phys. Chem.* **91**, 2513 (1987).
¹¹J. K. Gregory and D. C. Clary, *J. Chem. Phys.* **102**, 7817 (1995).
¹²J. K. Gregory and D. C. Clary, *J. Chem. Phys.* **103**, 8924 (1995).
¹³Y. Wang, B. J. Braams, J. M. Bowman, S. Carter, and D. P. Tew, *J. Chem. Phys.* **128**, 224314 (2008).
¹⁴A. Viel, M. D. Coutinho-Neto, and U. Manthe, *J. Chem. Phys.* **126**, 024308 (2007).
¹⁵W. H. Miller, *J. Chem. Phys.* **62**, 1899 (1975).
¹⁶D. G. Truhlar and A. Kuppermann, *J. Am. Chem. Soc.* **93**, 1840 (1971).
¹⁷C. G. Callan, Jr. and S. Coleman, *Phys. Rev. D* **16**, 1762 (1977).
¹⁸D. Chandler and P. G. Wolynes, *J. Chem. Phys.* **74**, 4078 (1981).
¹⁹S. Andersson, G. Nyman, A. Arnaldsson, U. Manthe, and H. Jónsson, *J. Phys. Chem. A* **113**, 4468 (2009).
²⁰J. B. Rommel, T. P. M. Goumans, and J. Kästner, *J. Chem. Theory Comput.* **7**, 690 (2011).
²¹J. B. Rommel and J. Kästner, *J. Chem. Phys.* **134**, 184107 (2011).
²²J. S. Cao and G. A. Voth, *J. Chem. Phys.* **105**, 6856 (1996).
²³N. Makri and W. H. Miller, *J. Chem. Phys.* **91**, 4026 (1989).
²⁴W. Siebrand, Z. Smedarchina, M. Z. Zgierski, and A. Fernández-Ramos, *Int. Rev. Phys. Chem.* **18**, 5 (1999).
²⁵V. A. Benderskii, E. V. Vetoshkin, L. von Laue, and H. P. Trommsdorff, *Chem. Phys.* **219**, 143 (1997).
²⁶V. A. Benderskii, V. I. Goldanskii, and D. E. Makarov, *Phys. Rep.* **233**, 195 (1993).
²⁷V. A. Benderskii, E. V. Vetoshkin, S. Y. Grebenshchikov, L. von Laue, and H. P. Trommsdorff, *Chem. Phys.* **219**, 119 (1997).
²⁸M. I. Katsnelson, M. van Schilfgaarde, V. P. Antropov, and B. N. Harmon, *Phys. Rev. A* **54**, 4802 (1996).

²⁹Z. Smedarchina, W. Siebrand, and M. Z. Zgierski, *J. Chem. Phys.* **103**, 5326 (1995).
³⁰Z. Smedarchina, W. Siebrand, and M. Z. Zgierski, *J. Chem. Phys.* **104**, 1203 (1996).
³¹Z. Smedarchina, W. Caminati, and F. Zerbetto, *Chem. Phys. Lett.* **237**, 279 (1995).
³²K. Yagi, T. Taketsugu, and K. Hirao, *J. Chem. Phys.* **115**, 10647 (2001).
³³G. S. Iroshnikov and L. P. Sukhanov, *Opt. Spectrosc.* **93**, 509 (2002).
³⁴G. S. Iroshnikov and L. P. Sukhanov, *Opt. Spectrosc.* **97**, 714 (2004).
³⁵G. Mil'nikov and H. Nakamura, *Phys. Chem. Chem. Phys.* **10**, 1374 (2008).
³⁶G. V. Mil'nikov and H. Nakamura, *J. Chem. Phys.* **115**, 6881 (2001).
³⁷G. V. Mil'nikov, K. Yagi, T. Taketsugu, H. Nakamura, and K. Hirao, *J. Chem. Phys.* **119**, 10 (2003).
³⁸G. V. Mil'nikov, and H. Nakamura, *J. Chem. Phys.* **122**, 124311 (2005).
³⁹C. S. Tautermann, A. F. Voegelé, T. Loerting, and K. R. Liedl, *J. Chem. Phys.* **117**, 1967 (2002).
⁴⁰C. S. Tautermann, A. F. Voegelé, T. Loerting, and K. R. Liedl, *J. Chem. Phys.* **117**, 1962 (2002).
⁴¹J. O. Richardson and S. C. Althorpe, *J. Chem. Phys.* **134**, 054109 (2011).
⁴²J. O. Richardson, S. C. Althorpe, and D. J. Wales, *J. Chem. Phys.* **135**, 124109 (2011).
⁴³T. Kawatsu and S. Miura, *J. Phys. Conf. Ser.* **454**, 012030 (2013).
⁴⁴Z. Smedarchina, W. Siebrand, and A. Fernández-Ramos, *J. Chem. Phys.* **137**, 224105 (2012).
⁴⁵R. Meana-Pañeda, D. G. Truhlar, and A. Fernández-Ramos, *J. Chem. Theory Comput.* **6**, 6 (2010).
⁴⁶W. S. Benedict and E. K. Plyler, *Can. J. Phys.* **35**, 1235 (1957).
⁴⁷E. Schnabel, T. Törring, and W. Wilke, *Z. Phys.* **188**, 167 (1965).
⁴⁸Y. Ootani and T. Taketsugu, *J. Comput. Chem.* **33**, 60 (2012).
⁴⁹T. Rajamäki, M. Kállay, J. Noga, P. Valiron, and L. Halonen, *Mol. Phys.* **102**, 2297 (2004).
⁵⁰T. Rajamäki, A. Miani, and L. Halonen, *J. Chem. Phys.* **118**, 10929 (2003).
⁵¹M. Neff and G. Rauhut, *Spectrochim. Acta A* **119**, 100 (2014).
⁵²T. Kashiwa, Y. Ohnuki, and M. Suzuki, *Path Integral Methods* (Clarendon Press, Oxford, 1997).
⁵³C. Y. Zhu, R. H. Byrd, P. H. Lu, and J. Nocedal, *ACM Trans. Math. Soft.* **23**, 550 (1997).
⁵⁴R. H. Byrd, P. H. Lu, J. Nocedal, and C. Y. Zhu, *SIAM J. Sci. Comput.* **16**, 1190 (1995).
⁵⁵M. R. Pastrana, L. A. M. Quintales, J. Brandão, and A. J. C. Varandas, *J. Phys. Chem.* **94**, 8073 (1990).
⁵⁶M. Page and J. W. McIver, Jr., *J. Chem. Phys.* **88**, 922 (1988).
⁵⁷See <http://www.netlib.org/lapack/lapacke.html> for The LAPACK; C interface to LAPACK library.
⁵⁸M. W. Schmidt, K. K. Baldrige, J. A. Boatz, S. T. Elbert, M. S. Gordon, J. H. Jensen, S. Koseki, N. Matsunaga, K. A. Nguyen, S. J. Su, T. L. Windus, M. Dupuis, and J. A. Montgomery, *J. Comput. Chem.* **14**, 1347 (1993).
⁵⁹C. C. J. Roothaan, *Rev. Modern Phys.* **23**, 69 (1951).
⁶⁰C. Möller and M. S. Plesset, *Phys. Rev.* **46**, 618 (1934).
⁶¹R. Krishnan, J. S. Binkley, R. Seeger, and J. A. Pople, *J. Chem. Phys.* **72**, 650 (1980).
⁶²T. Clark, J. Chandrasekhar, G. W. Spitznagel, and P. V. Schleyer, *J. Comput. Chem.* **4**, 294 (1983).
⁶³M. J. Frisch, J. A. Pople, and J. S. Binkley, *J. Chem. Phys.* **80**, 3265 (1984).
⁶⁴P. C. Hariharan and J. A. Pople, *Theor. Chim. Acta* **28**, 213 (1973).
⁶⁵R. Ditchfield, W. J. Hehre, and J. A. Pople, *J. Chem. Phys.* **54**, 724 (1971).
⁶⁶W. J. Hehre, R. Ditchfield, and J. A. Pople, *J. Chem. Phys.* **56**, 2257 (1972).
⁶⁷A. Schaefer, C. Huber, and R. Ahlrichs, *J. Chem. Phys.* **100**, 5829 (1994).
⁶⁸A. Schaefer, H. Horn, and R. Ahlrichs, *J. Chem. Phys.* **97**, 2571 (1992).
⁶⁹V. Špirko, *J. Mol. Spectrosc.* **101**, 30 (1983).
⁷⁰J. H. Callomon, E. Hirota, K. Kuchitsu, W. J. Lafferty, A. G. Maki, and C. S. Fote, *Inorganic Molecules in Landolt-Börnstein, Numerical Data and Functional Relationships in Science and Technology. Group II: Atomic and Molecular Physics*, edited by K.-H. Hellwege and A. M. Hellwege (Springer-Verlag, Berlin, 1976), p. 84.